Online Research @ Cardiff

This is an Open Access document downloaded from ORCA, Cardiff University's institutional repository: https://orca.cardiff.ac.uk/id/eprint/135322/

This is the author's version of a work that was submitted to / accepted for publication.

Citation for final published version:

Mihai, L. Angela ORCID: https://orcid.org/0000-0003-0863-3729 and Goriely, Alain 2020. A pseudo-anelastic model for stress softening in liquid crystal elastomers. Proceedings of the Royal Society A: Mathematical, Physical and Engineering Sciences 476 (2243) , 20200558. 10.1098/rspa.2020.0558 file

Publishers page: https://doi.org/10.1098/rspa.2020.0558
<https://doi.org/10.1098/rspa.2020.0558>

Please note:
Changes made as a result of publishing processes such as copy-editing, formatting and page numbers may not be reflected in this version. For the definitive version of this publication, please refer to the published source. You are advised to consult the publisher's version if you wish to cite this paper.

This version is being made available in accordance with publisher policies. See
http://orca.cf.ac.uk/policies.html for usage policies. Copyright and moral rights for publications made available in ORCA are retained by the copyright holders.

information services
gwasanaethau gwybodaeth

PROCEEDINGS A

rspa.royalsocietypublishing.org

Research

Article submitted to journal

Subject Areas:
applied mathematics, mathematical modelling, mechanics

Keywords:
liquid crystals, nematic solids, large deformation, stress softening, residual strain, cyclic loads

Author for correspondence:
L. Angela Mihai
e-mail: MihaiLA@cardiff.ac.uk

THE ROYAL SOCIETY
PUBLISHING

A pseudo-anelastic model for stress softening in liquid crystal elastomers

L. Angela Mihai[1] and Alain Goriely[2]

[1]School of Mathematics, Cardiff University, Senghennydd Road, Cardiff, CF24 4AG, UK
[2]Mathematical Institute, University of Oxford, Woodstock Road, Oxford, OX2 6GG, UK

Liquid crystal elastomers exhibit stress softening with residual strain under cyclic loads. Here, we model this phenomenon by generalising the classical pseudo-elastic formulation of the Mullins effect in rubber. Specifically, we modify the neoclassical strain-energy density of liquid crystal elastomers, depending on the deformation and the nematic director, by incorporating two continuous variables that account for stress softening and the associated set strain. As the material behaviour is governed by different forms of the strain-energy density on loading and unloading, the model is referred to as pseudo-anelastic. We then analyse qualitatively the mechanical responses of the material under cyclic uniaxial tension, which is easier to reproduce in practice, and further specialise the model in order to calibrate its parameters to recent experimental data at different temperatures. The excellent agreement between the numerical and experimental results confirms the suitability of our approach. Since the pseudo-energy function is controlled by the strain-energy density for the primary deformation, it is valid also for materials under multiaxial loads. Our study is relevant to mechanical damping applications and serves as a motivation for further experimental tests.

1. Introduction

Liquid crystalline solids are advanced manufactured materials combining the elasticity of rubber with the self-organisation of liquid crystals [16,27]. They consist of cross-linked networks of polymeric chains containing liquid crystal mesogens, and are capable of relatively large deformations, which arise spontaneously and reversibly under external stimuli (heat, light, solvents, electric or magnetic field) [17,35,38,48,64,75,77,79,85].

© The Authors. Published by the Royal Society under the terms of the Creative Commons Attribution License http://creativecommons.org/licenses/by/4.0/, which permits unrestricted use, provided the original author and source are credited.

Recent experimental studies have revealed softening effects under repeated tensile loading of nematic liquid crystal elastomer (NLCE) samples at different temperatures [5,49]. Specifically, a hysteretic response during unloading after loading in uniaxial tension was documented, whereby the stress on unloading was significantly less than that on loading at the same strain. In addition, after loading and subsequent unloading, the material did not return to its initial natural, stress-free configuration, but exhibited a residual strain. In contrast, LCE stiffening under compressive loads was recorded in [3]. Self-repair (or self-healing) was also observed experimentally in damaged LCEs [78].

Softening under repeated loading and unloading of rubber where filler particles (e.g., carbon black) are dispersed in the polymer network was initially obtained by Bouasse & Carriére (1903) [11] and is known as the *Mullins effect* [55–59]. This phenomenon is reversible since the material can 'heal' through re-cross-linking of network junctions at sufficiently high temperature [55,61,69,70]. A comprehensive study of filled polymers and their industrial applications is provided by the monograph [41]. Due to its industrial relevance, the Mullins effect has attracted considerable attention. Within the theoretical framework of large-strain finite elasticity, several constitutive models have been proposed. In [86], the rubber material was treated as a mixture of two macromolecular networks with different reference configurations. The model, which is valid when scission is caused by sufficiently large deformations, was refined in [66] and applied to specific equilibrium problems in [65]. A constitutive framework for the response of rubber that undergoes temperature-induced scission and re-cross-linking was developed in [87,88]. In [36], the Mullins effect in uniaxial tension was studied and used to describe the transverse vibration of a rubber string which was stretched repeatedly. Softening under different deformations than uniaxial tension was considered in [23,37,46]. Three-dimensional two-phase models were formulated in [6,32]. In [71], a phenomenological micromechanical model was devised starting from a polymeric network in which filler particles were treated as rigid spheres connected by two different types of chains, elastic or breakable. The efficiency of this model in describing three-dimensional inhomogeneous deformations was further demonstrated in [72]. In [15], the model was extended to incorporate healing. A mesoscopic model that describes the Mullins effect in rubber-like solids based on the notion of limiting chain extensibility associated with the Gent hyperelastic model was presented in [33,34]. In [40,63], a macroscopic *pseudo-elastic* model was introduced to account for stress softening by incorporating a continuous damage parameter into the hyperelastic strain-energy function for rubber. This material model comprises two different forms of the strain-energy density on loading and unloading, respectively, such that its mechanical behaviour can be treated within the elasticity framework, while loading-unloading cycles involve energy dissipation. In [24], the phenomenological pseudo-elastic strain-energy function was modified to account for both stress softening and the associated set strain. A particular version of this model was treated in [67]. An extensive survey on modelling approaches for the Mullins effect can be found in [22]. More recent experimental results are recorded in [42,44]. It is worth mentioning that Mullins-like effects have also been observed during experimental tests performed on certain soft tissues (e.g., arteries, skin, lungs, brain), where loading-unloading cycles are generally performed several times before the stress-strain relationship becomes repeatable. The procedure is known as *preconditioning* [12,25,30,60].

For ideal monodomain nematic solids, where the mesogens are aligned throughout the material, a general constitutive formulation is provided by the phenomenological neoclassical strain-energy function proposed in [10,81,84]. This model is based on the molecular network theory of rubber elasticity [73], and its parameters are directly measurable experimentally or derived from macroscopic shape changes [82,83]. Nematic monodomains can be formed from polydomains, which are generally isotropic, through stretching during the final cross-linking, or by cooling from the isotropic to the nematic phase under an external stress field [14,39]. For nematic polydomains, where the mesogens are separated into many domains, such that in every domain they are aligned along a local director, in [8,9], it was assumed that each domain has the same strain-energy density as a monodomain. However, similarly to the case of rubber elasticity,

the neoclassical theory requires modifications in order to accommodate material behaviours observed in certain experiments [45]. Extensions to nematic strain-energy densities based on classical hyperelastic models (e.g., Money-Rivlin, Gent, Ogden) are discussed in [1,2,21]. More general continuum mechanical theories are presented in [4,90].

In this study, we combine the neoclassical framework with the pseudo-elasticity theory proposed in [24,63] to construct a *phenomenological model* for NLCEs that captures stress softening and residual strain inelastic responses under repeated loads. In general, these responses are interpreted as being due to changes in the microstructural texture or viscoelasticity, but we do not consider microstructural or time-dependent effects here. In Section 2, we recall the neoclassical modelling strategy where we adopt the isotropic phase at high temperature as the reference configuration [13,18–21], rather than the nematic phase in which the cross-linking was produced [4,10,76,80,81,84,90]. Our choice is phenomenologically motivated by the multiplicative decomposition of the deformation gradient from the reference configuration to the current configuration into an elastic distortion followed by a natural (stress free) shape change. This multiplicative decomposition is similar to those found in the constitutive theories of thermoelasticity, elastoplasticity, and growth [31,43], but it is fundamentally different as, for LCEs, the stress-free geometrical change is superposed on the elastic deformation, which is applied directly to the reference state. The elastic stresses can then be used to analyse the final deformation where the particular geometry also plays a role. To formulate the pseudo-energy function, in Section 3, we modify the one-term (neo-Hookean-based) neoclassical strain-energy density, which characterises the NLCE material on primary loading from the undeformed state, through the incorporation of two additional variables that account for stress softening and residual strain on unloading, respectively. Because the material behaviour is governed by different forms of the strain-energy density on loading and unloading, and depends on both the deformation and the nematic director, the model is referred to as *pseudo-anelastic*. In Section 4, we analyse qualitatively the inelastic responses of the material in cyclic uniaxial tension. The scope of these two sections is to introduce the theoretical principles and present the general strategy for the pseudo-anelastic modelling in a manner that is mathematically and mechanically transparent. Carefully extending the one-term neoclassical model to the pseudo-anelastic form is the best way to illuminate the key aspect of the new approach. Following the general principles, other strain-energy functions could also be constructed if required by the experimental data, albeit with more complicated calculations due to additional nonlinearities. In Section 5, we select a pseudo-anelastic extension of Ogden-type and adjust its parameters to recent experimental data provided in [49]. However, for different experimental measurements, different strain-energy functions could better capture the observed mechanical behaviour, and the choice is not unique in general. In Section 6, we draw concluding remarks.

2. An ideal liquid crystal elastomer

The neoclassical strain-energy density function describing an ideal nematic liquid crystal elastomer (NLCE) takes the general form

$$W^{(nc)}(\mathbf{F},\mathbf{n}) = W(\mathbf{A}), \tag{2.1}$$

where $\mathbf{F}$ denotes the deformation gradient from the isotropic state, $\mathbf{n}$ is a unit vector field, known as the *director*, and $W(\mathbf{A})$ represents the strain-energy density of the isotropic polymer network, depending only on the (local) elastic deformation tensor $\mathbf{A}$. The tensors $\mathbf{F}$ and $\mathbf{A}$ satisfy the relation (see Figure 1)

$$\mathbf{F} = \mathbf{G}\mathbf{A}, \tag{2.2}$$

where

$$\mathbf{G} = a^{1/3}\mathbf{n}\otimes\mathbf{n} + a^{-1/6}\left(\mathbf{I} - \mathbf{n}\otimes\mathbf{n}\right) = a^{-1/6}\mathbf{I} + \left(a^{1/3} - a^{-1/6}\right)\mathbf{n}\otimes\mathbf{n}, \tag{2.3}$$

is the spontaneous deformation tensor defining a change of frame of reference from the isotropic phase to a nematic phase. This tensor is symmetric, i.e., $\mathbf{G} = \mathbf{G}^T$ (where the superscript "T"

denotes the transpose operator), but the elastic tensor $\mathbf{A}$ may not be symmetric in general. In (2.3), $a>0$ is the temperature-dependent stretch parameter, $\otimes$ denotes the usual tensor product of two vectors, and $\mathbf{I}=\mathrm{diag}(1,1,1)$ is the identity tensor. Here, it is assumed that a is spatially-independent (i.e., no differential swelling). For an ideal nematic solid, the 'anisotropy' ratio $r=a^{1/3}/a^{-1/6}=a^{1/2}$ is the same in all directions. In the nematic phase, both the cases with $r>1$ (prolate molecules) and $r<1$ (oblate molecules) are possible, while when $r=1$, the energy function reduces to that of an isotropic hyperelastic material [17].

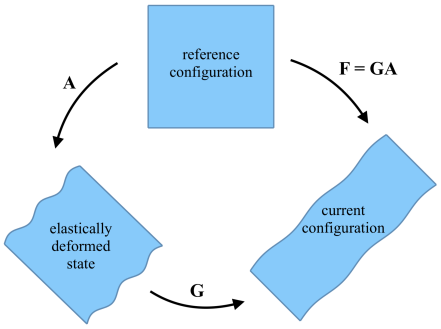

Figure 1. Schematic of the composite deformation of a nematic solid.

In (2.1), the elastic strain-energy function W is minimised by any deformation satisfying $\mathbf{A}\mathbf{A}^T=\mathbf{I}$ [62,74], whereas the corresponding nematic strain-energy $W^{(nc)}$ is minimised by any deformation satisfying $\mathbf{F}\mathbf{F}^T=\mathbf{G}^2$. Hence, every pair $(\mathbf{GR},\mathbf{n})$, with $\mathbf{R}$ an arbitrary rigid-body rotation (i.e., $\mathbf{R}^{-1}=\mathbf{R}^T$ and $\det\mathbf{R}=1$), is a natural (i.e., stress free) state for this material model. By (2.3), the following identity holds

$$\mathbf{R}^T\mathbf{G}\mathbf{R}=a^{-1/6}\mathbf{I}+\left(a^{1/3}-a^{-1/6}\right)\left(\mathbf{R}^T\mathbf{n}\right)\otimes\left(\mathbf{R}^T\mathbf{n}\right). \tag{2.4}$$

The director $\mathbf{n}$ is an observable (spatial) quantity. Denoting by $\mathbf{n}_0$ the reference orientation of the local director corresponding to the cross-linking state, $\mathbf{n}$ and $\mathbf{n}_0$ may differ both by a rotation and a change in r. Many macroscopic deformations of nematic elastomers induce a director re-orientation whereby the director aligns in the direction of the largest principal stretch associated with the deformation. The strain energy given by (2.1) satisfies the following conditions, which are inherited from isotropic finite elasticity [51]:

Material objectivity. This states that constitutive equations must be invariant under changes of frame of reference. It requires that the scalar strain-energy function $W^{(nc)}(\mathbf{F},\mathbf{n})$ is unaffected by a superimposed rigid-body transformation (which involves a change of position) after deformation, i.e., $W^{(nc)}\left(\mathbf{R}^T\mathbf{F},\mathbf{R}^T\mathbf{n}\right)=W^{(nc)}\left(\mathbf{F},\mathbf{n}\right)$, where $\mathbf{R}\in SO(3)$ is a proper orthogonal tensor (rotation). Note that, as $\mathbf{n}$ is defined with respect to the deformed configuration, it transforms when this configuration is rotated, whereas $\mathbf{n}_0$ does not [29]. Material objectivity is guaranteed by defining strain-energy functions in terms of the scalar invariants. Indeed, by the material frame indifference of W,

$$W\left(\mathbf{R}^T\mathbf{A}\right)=W(\mathbf{A}), \tag{2.5}$$

and by (2.2),

$$\mathbf{R}^T\mathbf{F}=\left(\mathbf{R}^T\mathbf{G}\mathbf{R}\right)\left(\mathbf{R}^T\mathbf{A}\right). \tag{2.6}$$

Then, (2.1), (2.4), (2.5) and (2.6) imply

$$W^{(nc)}\left(\mathbf{R}^T\mathbf{F},\mathbf{R}^T\mathbf{n}\right)=W\left(\mathbf{R}^T\mathbf{A}\right)=W(\mathbf{A})=W^{(nc)}(\mathbf{F},\mathbf{n}). \tag{2.7}$$

Material isotropy. This requires that the strain-energy density is unaffected by a superimposed rigid-body transformation prior to deformation, i.e., $W^{(nc)}(\mathbf{FQ}, \mathbf{n}) = W^{(nc)}(\mathbf{F}, \mathbf{n})$, where $\mathbf{Q} \in SO(3)$. Note that, as $\mathbf{n}$ is defined with respect to the deformed configuration, it does not change when the reference configuration is rotated, whereas $\mathbf{n}_0$ does [29]. For isotropic materials, the strain-energy function is a symmetric function of the principal stretch ratios $\{\lambda_i\}_{i=1,2,3}$ of $\mathbf{F}$. The squares of the principal stretches, $\{\lambda_i^2\}_{i=1,2,3}$, are the eigenvalues of the deformation tensors $\mathbf{FF}^T$ and $\mathbf{F}^T\mathbf{F}$. This is because, as W is isotropic, i.e.,

$$W(\mathbf{A}) = W(\mathbf{AQ}), \tag{2.8}$$

and (2.2) holds, it follows that

$$\mathbf{FQ} = \mathbf{G}\,(\mathbf{AQ})\,. \tag{2.9}$$

Hence, by (2.1), (2.8) and (2.9),

$$W^{(nc)}(\mathbf{FQ}, \mathbf{n}) = W(\mathbf{AQ}) = W(\mathbf{A}) = W^{(nc)}(\mathbf{F}, \mathbf{n}). \tag{2.10}$$

For an homogeneous isotropic incompressible hyperelastic material described by the strain-energy function $W(\mathbf{A})$, the Cauchy stress tensor (representing the internal force per unit of deformed area acting within the deformed solid) takes the form [31,50,62,74]

$$\mathbf{T} = (\det \mathbf{A})^{-1}\,\frac{\partial W}{\partial \mathbf{A}}\mathbf{A}^T - p\mathbf{I} = -p\mathbf{I} + \beta_1\mathbf{B} + \beta_{-1}\mathbf{B}^{-1}, \tag{2.11}$$

where p denotes the Lagrange multiplier for the incompressibility constraint $\det \mathbf{A} = 1$,

$$\beta_1 = 2\frac{\partial W}{\partial I_1}, \qquad \beta_{-1} = -2\frac{\partial W}{\partial I_2} \tag{2.12}$$

are material parameters, $\mathbf{B} = \mathbf{AA}^T$ is the left Cauchy-Green elastic deformation tensor, and I_1, I_2 are its first two principal invariants ($I_3 = \det \mathbf{B} = 1$ for incompressibility).

The associated first Piola-Kirchhoff (PK) stress tensor (representing the internal force per unit of undeformed area acting within the deformed solid) is equal to

$$\mathbf{P} = \mathbf{T}\,\mathrm{Cof}(\mathbf{A}) = \mathbf{TA}^{-T}. \tag{2.13}$$

where $\mathrm{Cof}(\mathbf{A}) = (\det \mathbf{A})\,\mathbf{A}^{-T}$ is the cofactor of $\mathbf{A}$.

For the associated nematic elastomers described by (2.1), when the director is free to rotate, using the multiplicative decomposition (2.2), the Cauchy stress tensor takes the form [52]

$$\mathbf{T}^{(nc)} = J^{-1}\frac{\partial W^{(nc)}}{\partial \mathbf{F}}\mathbf{F}^T - p^{(nc)}\mathbf{I} = J^{-1}\mathbf{G}^{-1}\frac{\partial W}{\partial \mathbf{A}}\mathbf{A}^T\mathbf{G} - p^{(nc)}\mathbf{I} = J^{-1}\mathbf{G}^{-1}\mathbf{TG}, \tag{2.14}$$

where $\mathbf{T}$ is the Cauchy stress defined by (2.11), $J = \det \mathbf{F}$, and the scalar $p^{(nc)}$ (the hydrostatic pressure) represents the Lagrange multiplier for the internal constraint $\det \mathbf{F} = 1$.

The Cauchy stress tensor $\mathbf{T}^{(nc)}$ given by (2.14) is not symmetric in general [4,68,90], and in addition, the following condition is assumed [4,90],

$$\frac{\partial W^{(nc)}}{\partial \mathbf{n}}(\mathbf{F}, \mathbf{n}) = \mathbf{0}. \tag{2.15}$$

Equivalently, by the principle of material objectivity stating that constitutive equations must be invariant under changes of frame of reference (see [4] for details),

$$\left(\mathbf{T}^{(nc)T} - \mathbf{T}^{(nc)}\right)\mathbf{n} = \mathbf{0}. \tag{2.16}$$

The first Piola-Kirchhoff (PK) stress tensor for the nematic material is then

$$\mathbf{P}^{(nc)} = \mathbf{T}^{(nc)}\mathrm{Cof}(\mathbf{F}) = \mathbf{G}^{-1}\mathbf{TA}^{-T} = \mathbf{G}^{-1}\mathbf{P}, \tag{2.17}$$

where $\mathbf{P}$ is the first Piola-Kirchhoff stress given by (2.13).

3. The pseudo-energy function

In this section, we construct a *pseudo-anelastic* energy function to capture stress softening with associated residual strain in nematic elastomers under cyclic loads (see also [7,47,89]). In its general form, this function builds directly on the neoclassical model, which depends on both the strain and the nematic director, and is similar to the pseudo-elastic strain-energy function accounting for the Mullins effect in filled rubbers [24,63]. Therefore, we briefly recall the steps associated with the construction of a pseudo-elastic energy function first, and then extend the method to nematic materials.

(a) The pseudo-elastic strain-energy function

Based on the notion of *pseudo-elasticity* introduced in [30], the Mullins effect of rubber can be captured by modifying the strain-energy function for an isotropic incompressible hyperelastic material to account for stress softening and residual strain. A general form of the *pseudo-elastic energy function* is given as follow [24],

$$\widetilde{W}(\alpha_1,\alpha_2,\alpha_3,\eta_0,\eta_1)=\eta_0 W_0(\alpha_1,\alpha_2,\alpha_3)+(1-\eta_1)\,W_1(\alpha_1,\alpha_2,\alpha_3)+\phi_0(\eta_0)+\phi_1(\eta_1). \tag{3.1}$$

In this equation, $W_0(\alpha_1,\alpha_2,\alpha_3)$ is a hyperelastic strain-energy function of the ordered principal stretch ratios $0<\alpha_3\le\alpha_2\le\alpha_1$, representing the singular values of the elastic deformation gradient $\mathbf{A}$; $\phi_0(\eta_0)$ is a function of the 'damage' (or 'softening') scalar variable η_0 associated with the softening effect; $\phi_1(\eta_1)$ is a function of the 'residual strain' scalar variable η_1 associated with set strain effect; and $W_1(\alpha_1,\alpha_2,\alpha_3)$ is an auxiliary function. The pseudo-energy function described by (3.1) is required to satisfy the material objectivity condition [63].

On the primary loading path, i.e., loading from the undeformed state, the material is fully determined by the elastic strain-energy density. Therefore, the variables η_0 and η_1 are inactive on loading, where they are set equal to a given constant value, and active on unloading, where they change the material properties. For simplicity, it is assumed that

$$\frac{\partial\widetilde{W}}{\partial\eta_0}(\alpha_1,\alpha_2,\alpha_3,\eta_0,\eta_1)=0,\qquad \frac{\partial\widetilde{W}}{\partial\eta_1}(\alpha_1,\alpha_2,\alpha_3,\eta_0,\eta_1)=0. \tag{3.2}$$

These equations determine η_0 and η_1 implicitly in terms of the stretch ratios $\{\alpha_i\}_{i=1,2,3}$.

For example, we consider the neo-Hookean (NH) strain-energy function (see also [62])

$$W_0(\alpha_1,\alpha_2,\alpha_3)=\frac{\mu}{2}\left(\alpha_1^2+\alpha_2^2+\alpha_3^2-3\right), \tag{3.3}$$

where $\mu>0$ represents the constant shear modulus at small strain, and $\{\alpha_i^2\}_{i=1,2,3}$ are the principal eigenvalues of the Cauchy-Green tensors $\mathbf{B}=\mathbf{A}\mathbf{A}^T$ and $\mathbf{C}=\mathbf{A}^T\mathbf{A}$.

We can define the auxiliary function by [24]

$$W_1(\alpha_1,\alpha_2,\alpha_3)=\frac{1}{2}\left[C_1\left(\alpha_1^2-1\right)+C_2\left(\alpha_2^2-1\right)+C_3\left(\alpha_3^2-1\right)\right], \tag{3.4}$$

where $\{C_i\}_{i=1,2,3}$ are constants that can be adjusted to data.

The great advantage of this approach is that, despite the fact that the pseudo-elastic model described by (3.1) takes different forms on loading and unloading, it can be studied by the usual methods of finite elasticity on each path.

(b) The pseudo-anelastic energy function for liquid crystal elastomers

Combining the neoclassical and pseudo-elasticity theories, we extend the formulation of a pseudo-energy function to nematic elastomers as follows,

$$\begin{aligned}\widetilde{W}^{(nc)}(\lambda_1,\lambda_2,\lambda_3,\mathbf{n},\eta_0,\eta_1)=\eta_0 W_0^{(nc)}(\lambda_1,\lambda_2,\lambda_3,\mathbf{n})+\phi_0^{(nc)}(\eta_0)\\ +(1-\eta_1)\,W_1^{(nc)}(\lambda_1,\lambda_2,\lambda_3,\mathbf{n})+\phi_1^{(nc)}(\eta_1),\end{aligned} \tag{3.5}$$

where

$$W_0^{(nc)}(\lambda_1,\lambda_2,\lambda_3,\mathbf{n})=\frac{\mu}{2}\left\{a^{1/3}\left[\sum_{i=1}^{3}\lambda_i^2-\left(1-a^{-1}\right)\sum_{i=1}^{3}\lambda_i^2\left(\mathbf{e}_i\cdot\mathbf{n}\right)^2\right]-3\right\} \tag{3.6}$$

represents the neoclassical strain-energy function defined by (2.1), with the NH strain-energy density of the elastic network given by (3.3), $\{\lambda_i^2\}_{i=1,2,3}$ and $\{\mathbf{e}_i\}_{i=1,2,3}$ denote, respectively, the principal eigenvalues and principal eigenvectors of the deformation tensors $\mathbf{F}\mathbf{F}^T$ and $\mathbf{F}^T\mathbf{F}$ (see also [51,52]), and

$$W_1^{(nc)}(\lambda_1,\lambda_2,\lambda_3,\mathbf{n})=\frac{1}{2}a^{1/3}\left[\sum_{i=1}^{3}C_i\lambda_i^2-\left(1-a^{-1}\right)\sum_{i=1}^{3}C_i\lambda_i^2\left(\mathbf{e}_i\cdot\mathbf{n}\right)^2\right]-\frac{C_1+C_2+C_3}{2} \tag{3.7}$$

is an auxiliary nematic function based on the function given by (3.4), with α_1 replaced by $\lambda_1 a^{-1/3}$ and α_i replaced by $\lambda_i a^{1/6}$, $i=2,3$. We also assume

$$\frac{\partial\widetilde{W}^{(nc)}}{\partial\eta_0}(\lambda_1,\lambda_2,\lambda_3,\mathbf{n},\eta_0,\eta_1)=0,\qquad \frac{\partial\widetilde{W}^{(nc)}}{\partial\eta_1}(\lambda_1,\lambda_2,\lambda_3,\mathbf{n},\eta_0,\eta_1)=0. \tag{3.8}$$

We call the material model described by (3.5) *pseudo-anelastic* as it takes different forms on loading and unloading, like the pseudo-elasticity model, but depends on the nematic director as well [26]. The associated Cauchy and first Piola-Kirchhoff stress tensors are calculated by similar formulae as given in (2.14) and (2.17), respectively, with $\widetilde{W}^{(nc)}$ instead of $W^{(nc)}$.

As the material is incompressible, i.e., $\lambda_1\lambda_2\lambda_3=\det\mathbf{F}=\det\mathbf{G}=1$, we have $\lambda_3=\lambda_1^{-1}\lambda_2^{-1}$, and given that the nematic director $\mathbf{n}$ can rotate freely, it follows that

$$W_0^{(nc)}(\lambda_1,\lambda_2,\mathbf{n})=\frac{\mu}{2}\left[a^{1/3}\left(\frac{\lambda_1^2}{a}+\lambda_2^2+\lambda_1^{-2}\lambda_2^{-2}\right)-3\right] \tag{3.9}$$

and

$$W_1^{(nc)}(\lambda_1,\lambda_2,\mathbf{n})=\frac{1}{2}a^{1/3}\left(\frac{C_1\lambda_1^2}{a}+C_2\lambda_2^2+C_3\lambda_1^{-2}\lambda_2^{-2}\right)-\frac{C_1+C_2+C_3}{2}. \tag{3.10}$$

Without loss of generality, we set $\eta_0=\eta_1=1$ when η_0 and η_1 are inactive, and take the functions $\phi_0^{(nc)}$ and $\phi_1^{(nc)}$ to satisfy, respectively, the conditions [24]

$$\phi_0^{(nc)}(1)=0,\qquad \phi_1^{(nc)}(1)=0. \tag{3.11}$$

Then, by (3.5) and (3.11),

$$\widetilde{W}^{(nc)}(\lambda_1,\lambda_2,\mathbf{n},1,1)=W_0^{(nc)}(\lambda_1,\lambda_2,\mathbf{n}), \tag{3.12}$$

where $W_0^{(nc)}(\lambda_1,\lambda_2,\mathbf{n})$, given by (3.9), represents the energy function of the perfectly elastic material, for which the loading and unloading paths are the same.

When η_0 and η_1 are active, assuming that equations (3.8) can be solved explicitly, we can write

$$\eta_0=\eta_0(\lambda_1,\lambda_2,\mathbf{n}),\qquad \eta_1=\eta_1(\lambda_1,\lambda_2,\mathbf{n}), \tag{3.13}$$

and then define the energy function on unloading as

$$\widetilde{w}^{(nc)}(\lambda_1,\lambda_2,\mathbf{n})=\widetilde{W}^{(nc)}(\lambda_1,\lambda_2,\mathbf{n},\eta_0(\lambda_1,\lambda_2,\mathbf{n}),\eta_1(\lambda_1,\lambda_2,\mathbf{n})). \tag{3.14}$$

If $\left(\lambda_1^{(m)},\lambda_2^{(m)}\right)$ are the values of (λ_1,λ_2) at which unloading is initiated, then

$$\eta_0\left(\lambda_1^{(m)},\lambda_2^{(m)},\mathbf{n}\right)=1,\qquad \eta_1\left(\lambda_1^{(m)},\lambda_2^{(m)},\mathbf{n}\right)=1. \tag{3.15}$$

By (3.8), the first derivatives of $\phi_0^{(nc)}$ and $\phi_1^{(nc)}$ with respect to η_0 and η_1, respectively, satisfy the following equations,

$$\frac{\mathrm{d}\phi_0^{(nc)}}{\mathrm{d}\eta_0}(\eta_0) = -W_0^{(nc)}(\lambda_1, \lambda_2, \mathbf{n}), \qquad \frac{\mathrm{d}\phi_1^{(nc)}}{\mathrm{d}\eta_1}(\eta_1) = W_1^{(nc)}(\lambda_1, \lambda_2, \mathbf{n}). \tag{3.16}$$

These implicitly define η_0 and η_1 in terms of λ_1, λ_2 and $\mathbf{n}$.

(c) Stress softening with residual strain in nematic elastomers

On the primary loading path, where $\eta_0 = \eta_1 = 1$, setting $\lambda_1 = \lambda_1^{(m)}$ and $\lambda_2 = \lambda_2^{(m)}$ the stretch ratios from which unloading begins, we have

$$\frac{\mathrm{d}\phi_0^{(nc)}}{\mathrm{d}\eta_0}(1) = -W_0^{(nc)}\left(\lambda_1^{(m)}, \lambda_2^{(m)}, \mathbf{n}\right), \qquad \frac{\mathrm{d}\phi_1^{(nc)}}{\mathrm{d}\eta_1}(1) = W_1^{(nc)}\left(\lambda_1^{(m)}, \lambda_2^{(m)}, \mathbf{n}\right). \tag{3.17}$$

After unloading, in the absence of a residual elastic deformation, such that $a^{-1/3}\lambda_1 = a^{1/6}\lambda_2 = 1$ and $\eta_1 = 1$, if $\eta_0^{(m)} = \eta_0\left(a^{1/3}, a^{-1/6}, \mathbf{n}\right)$ denotes the corresponding value of η_0, then

$$\frac{\mathrm{d}\phi_0^{(nc)}}{\mathrm{d}\eta_0}\left(\eta_0^{(m)}\right) = -W_0^{(nc)}\left(a^{1/3}, a^{-1/6}, \mathbf{n}\right) = 0. \tag{3.18}$$

In this case, the residual value of the pseudo-energy function when the material is fully unloaded is equal to

$$\phi_0^{(nc)}\left(\eta_0^{(m)}\right) = \widetilde{w}^{(nc)}\left(a^{1/3}, a^{-1/6}, \mathbf{n}\right) = \widetilde{W}^{(nc)}\left(a^{1/3}, a^{-1/6}, \mathbf{n}, \eta_0^{(m)}, 1\right). \tag{3.19}$$

We define

$$\varphi_0^{(nc)}(\eta_0) = \frac{\mathrm{d}\phi_0^{(nc)}}{\mathrm{d}\eta_0}(\eta_0) - \frac{\mathrm{d}\phi_0^{(nc)}}{\mathrm{d}\eta_0}(1), \tag{3.20}$$

which, by (3.17) and (3.18), at the beginning and the end of unloading, satisfies, respectively,

$$\varphi_0^{(nc)}(1) = 0, \qquad \varphi_0^{(nc)}\left(\eta_0^{(m)}\right) = W_0^{(nc)}\left(\lambda_1^{(m)}, \lambda_2^{(m)}, \mathbf{n}\right). \tag{3.21}$$

Integration of (3.20) gives

$$\phi_0^{(nc)}(\eta_0) = \int_1^{\eta_0} \varphi_0^{(nc)}(\zeta)\mathrm{d}\zeta + (1-\eta_0)\varphi_0^{(nc)}\left(\eta_0^{(m)}\right). \tag{3.22}$$

Furthermore,

$$\dot{\phi}_0^{(nc)}(\eta_0^{(m)}) = \left(1 - \eta_0^{(m)}\right)\dot{W}_0^{(nc)}\left(\lambda_1^{(m)}, \lambda_2^{(m)}, \mathbf{n}\right), \tag{3.23}$$

where the superposed "dot" denotes differentiation with respect to any deformation parameter that increases with loading (e.g., differentiation with respect to time). As $\eta_0^{(m)} \leq 1$, with equality only at the beginning of the primary loading, and since the stored energy on the primary loading path must increase, i.e., $\dot{W}_0^{(nc)}\left(\lambda_1^{(m)}, \lambda_2^{(m)}, \mathbf{n}\right) > 0$, by (3.23), it follows that $\dot{\phi}_0^{(nc)}\left(\eta_0^{(m)}\right) \geq 0$ [63].

A suitable choice for $\phi_0^{(nc)}(\eta_0)$ is given by the solution of

$$\frac{\mathrm{d}\phi_0^{(nc)}}{\mathrm{d}\eta_0}(\eta_0) = -\mu m\,\mathrm{erf}^{-1}\left(r(\eta_0 - 1)\right) - W_0^{(nc)}\left(\lambda_1^{(m)}, \lambda_2^{(m)}, \mathbf{n}\right), \tag{3.24}$$

where erf^{-1} is the inverse of the error function, and m and r are positive constants that can be adjusted to the data. By (3.16) and (3.24), we have

$$\eta_0(\lambda_1, \lambda_2, \mathbf{n}) = 1 - \frac{1}{r}\mathrm{erf}\left(\frac{1}{\mu m}\left[W_0^{(nc)}\left(\lambda_1^{(m)}, \lambda_2^{(m)}, \mathbf{n}\right) - W_0^{(nc)}\left(\lambda_1, \lambda_2, \mathbf{n}\right)\right]\right). \tag{3.25}$$

Since $\mathrm{erf}(0)=0$ and $\mathrm{erf}(\infty)=1$, for η_0 to be positive, we require $r>1$. The minimum value of this function is attained in the naturally deformed state, where $a^{-1/3}\lambda_1=a^{1/6}\lambda_2=1$, and is equal to

$$\eta_0^{(m)}=\eta_0\left(a^{1/3},a^{-1/6},\mathbf{n}\right)=1-\frac{1}{r}\mathrm{erf}\left(\frac{1}{\mu m}W_0^{(nc)}\left(\lambda_1^{(m)},\lambda_2^{(m)},\mathbf{n}\right)\right)>0. \tag{3.26}$$

In (3.26), $r\left(1-\eta_0^{(m)}\right)$ represents the probability that a random variable with normal distribution of mean 0 and variance $1/2$ lies between $-W_0^{(nc)}\left(\lambda_1^{(m)},\lambda_2^{(m)},\mathbf{n}\right)/(\mu m)$ and $W_0^{(nc)}\left(\lambda_1^{(m)},\lambda_2^{(m)},\mathbf{n}\right)/(\mu m)$.

When residual strain is present, on unloading, η_1 should be decreasing. A suitable form for this parameter is

$$\eta_1(\lambda_1,\lambda_2)=\frac{1}{\mathrm{erf}(1)}\mathrm{erf}\left(\left(\frac{W_0^{(nc)}(\lambda_1,\lambda_2,\mathbf{n})}{W_0^{(nc)}\left(\lambda_1^{(m)},\lambda_2^{(m)},\mathbf{n}\right)}\right)^p\right), \tag{3.27}$$

where $p\geq 1$ is a function of $W_0^{(nc)}\left(\lambda_1^{(m)},\lambda_2^{(m)},\mathbf{n}\right)$. The minimum value of this function is also attained when $a^{-1/3}\lambda_1=a^{1/6}\lambda_2=1$, and is equal to

$$\eta_1^{(m)}=\eta_1\left(a^{1/3},a^{-1/6},\mathbf{n}\right)=0. \tag{3.28}$$

The function $\phi_1^{(nc)}$ associated with the residual strain is defined implicitly in (3.16).

In particular, if $W_0^{(nc)}(\lambda_1,\lambda_2,\mathbf{n})$ is described by (3.9), then

$$\eta_0=1-\frac{1}{r}\mathrm{erf}\left(\frac{1}{2m}a^{1/3}\left[\frac{\left(\lambda_1^{(m)}\right)^2-\lambda_1^2}{a}+\left(\lambda_2^{(m)}\right)^2-\lambda_2^2+\left(\lambda_1^{(m)}\right)^{-2}\left(\lambda_2^{(m)}\right)^{-2}-\lambda_1^{-2}\lambda_2^{-2}\right]\right) \tag{3.29}$$

and

$$\eta_1=\frac{1}{\mathrm{erf}(1)}\mathrm{erf}\left(\left(\frac{\frac{\lambda_1^2}{a}+\lambda_2^2+\lambda_1^{-2}\lambda_2^{-2}-3}{\frac{\left(\lambda_1^{(m)}\right)^2}{a}+\left(\lambda_2^{(m)}\right)^2+\left(\lambda_1^{(m)}\right)^{-2}\left(\lambda_2^{(m)}\right)^{-2}-3}\right)^p\right). \tag{3.30}$$

Here, we have chosen the error function, erf, to express the variables η_0 and η_1, but this choice is not unique. For example, in [24], the hyperbolic tangent function is used instead.

4. Uniaxial tension

We analyse the mechanical behaviour of the pseudo-energy function defined by (3.5) in uniaxial tension, such that

$$\lambda_1=\lambda \qquad \text{and} \qquad \lambda_2=\lambda_3=\frac{1}{\sqrt{\lambda}}, \tag{4.1}$$

where $\lambda=a^{1/3}$ is the extension ratio for the natural deformation, and $\lambda/a^{1/3}-1$ is the elastic strain due to the tensile load (various definitions of the elastic strain for large deformations are presented in [50]). In this case, the equations given in (3.16) become, respectively,

$$\frac{\mathrm{d}\phi_0^{(nc)}}{\mathrm{d}\eta_0}(\eta_0)=-W_0^{(nc)}(\lambda,\mathbf{n}), \qquad \frac{\mathrm{d}\phi_1^{(nc)}}{\mathrm{d}\eta_1}(\eta_1)=W_1^{(nc)}(\lambda,\mathbf{n}), \tag{4.2}$$

where

$$W_0^{(nc)}(\lambda,\mathbf{n})=\frac{\mu}{2}\left[a^{1/3}\left(\frac{\lambda^2}{a}+2\lambda^{-1}\right)-3\right] \tag{4.3}$$

and

$$W_1^{(nc)}(\lambda,\mathbf{n})=\frac{1}{2}a^{1/3}\left[\frac{C_1\lambda^2}{a}+(C_2+C_3)\lambda^{-1}\right]-\frac{C_1+C_2+C_3}{2}. \tag{4.4}$$

We focus first on the case when only stress softening occurs, then we take also into account the associated residual strain.

(a) Stress softening

When η_0 is active and $\eta_1 = 1$, by (3.24) and (3.25), with the stretch ratios satisfying (4.1), we have

$$\frac{\mathrm{d}\phi_0^{(nc)}}{\mathrm{d}\eta_0}(\eta_0) = -\mu m \,\mathrm{erf}^{-1}\left(r(\eta_0 - 1)\right) - W_0^{(nc)}\left(\lambda^{(m)}, \mathbf{n}\right) \tag{4.5}$$

and

$$\eta_0(\lambda, \mathbf{n}) = 1 - \frac{1}{r}\mathrm{erf}\left(\frac{1}{\mu m}\left[W_0^{(nc)}\left(\lambda^{(m)}, \mathbf{n}\right) - W_0^{(nc)}(\lambda, \mathbf{n})\right]\right), \tag{4.6}$$

where $\lambda^{(m)}$ is the elastic stretch ratio at which unloading begins. By (4.3) and (4.6), we obtain

$$\eta_0(\lambda, \mathbf{n}) = 1 - \frac{1}{r}\mathrm{erf}\left(\frac{1}{2m}a^{1/3}\left[\frac{\left(\lambda^{(m)}\right)^2 - \lambda^2}{a} + 2\left(\lambda^{(m)}\right)^{-1} - 2\lambda^{-1}\right]\right). \tag{4.7}$$

Hence, by (3.26) and (4.3),

$$\eta_0^{(m)} = \eta_0(a^{1/3}, \mathbf{n}) = 1 - \frac{1}{r}\mathrm{erf}\left(\frac{1}{2m}\left[\frac{\left(\lambda^{(m)}\right)^2}{a^{2/3}} + 2\left(\lambda^{(m)}\right)^{-1}a^{1/3} - 3\right]\right). \tag{4.8}$$

We infer that:

(I) As $r > 1$ decreases, the difference between η_0 and 1 increases, i.e., damage increases;

(II) As $m > 0$ decreases, there is increasing damage at small strains, but the material response at small strain on repeated re-loading remains effectively unchanged. As $m > 0$ increases, there is decreasing damage at small strains, but the change in the material response at small strain increases upon subsequent re-loading compared to the undamaged state;

(III) As $a > 0$ decreases, damage increases at small strains, but the material response on repeated re-loading remains practically unchanged. As $a > 0$ increases, damage decreases at small strain, but the change in the material response increases upon further re-loading compared to the undamaged state.

This behaviour is illustrated numerically in Figures 2-4, where the first Piola-Kirchhoff stress takes the form

$$P_0^{(nc)} = a^{-1/3}P_0 = \eta_0\mu a^{1/3}\left(\frac{\lambda}{a} - \lambda^{-2}\right). \tag{4.9}$$

The corresponding Cauchy stress is equal to

$$T_0^{(nc)} = T_0 = \eta_0\mu a^{1/3}\left(\frac{\lambda^2}{a} - \lambda^{-1}\right). \tag{4.10}$$

In Figures 2-3, for $a = 1$, corresponding to the purely elastic case, and different values of r and m, respectively, we represent the scaled first Piola-Kirchhoff stress $P_0^{(nc)}/\mu$, given by (4.9), and the damage function η_0, defined by (4.7). These figures show that damage at small strains increases when r decreases, and also when m decreases, while the response at small strains increases upon repeated re-loading when m increases. In Figure 4, for nematic materials with different values of the parameter a, the scaled first Piola-Kirchhoff stress $P_0^{(nc)}/\mu$ and the damage function η_0 are shown when $r = 2$ and $m = 0.2$ are fixed. In this figure, damage at small strains increases when a decreases, and the response at small strains increases upon repeated re-loading when a increases.

More generally, when other deformation paths are considered, any pair of (λ_1, λ_2), such that $W_0^{(nc)}(\lambda_1, \lambda_2, \mathbf{n}) = W_0^{(nc)}\left(\lambda^{(m)}, \mathbf{n}\right)$ can be taken as the starting point for unloading instead of $\left(\lambda^{(m)}, 1/\sqrt{\lambda^{(m)}}\right)$. Then, if the value $W_0^{(nc)}\left(\lambda^{(m)}, \mathbf{n}\right)$ is fixed, the set of such pairs forms a

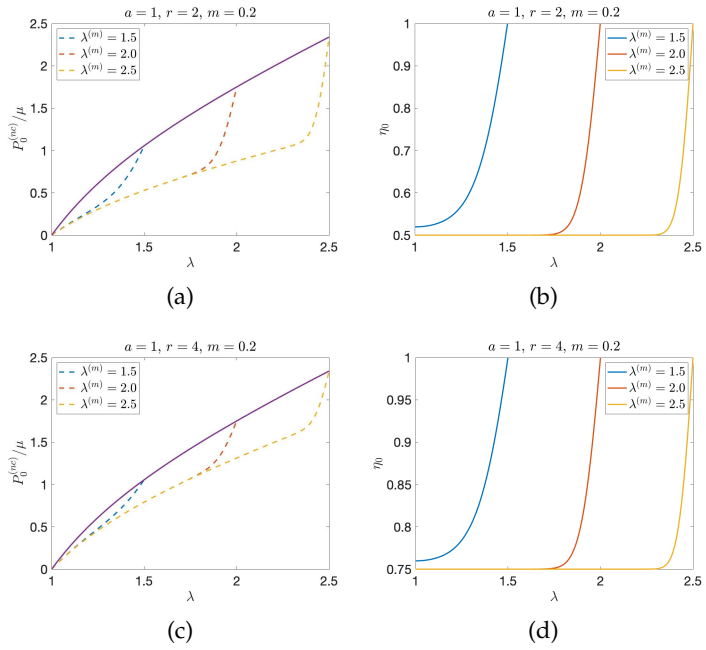

Figure 2. The effect of changing parameter r, showing: (a,c) The scaled values $P_0^{(nc)}/\mu$ of the first Piola-Kirchhoff stress given by (4.9) and (b,d) the damage function η_0 defined by (4.7) when $a = 1$ and $m = 0.2$. In (a,c), the solid curve is for the primary loading, and dashed curves for the unloading from different values of the maximum stretch ratio $\lambda^{(m)}$.

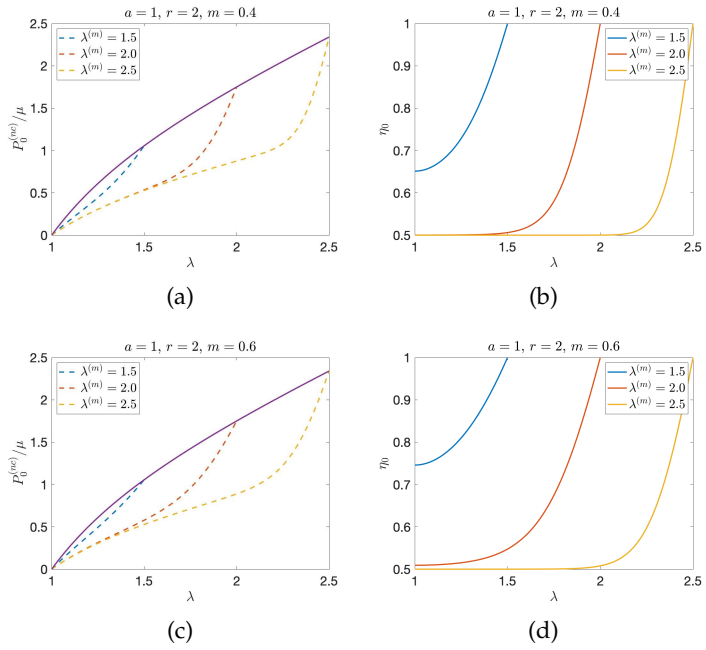

Figure 3. The effect of changing parameter m, showing: (a,c) The scaled values $P_0^{(nc)}/\mu$ of the first Piola-Kirchhoff stress given by (4.9) and (b,d) the damage function η_0 defined by (4.7) when $a = 1$ and $r = 2$. In (a,c), the solid curve is for the primary loading, and dashed curves for the unloading from different values of the maximum stretch ratio $\lambda^{(m)}$.

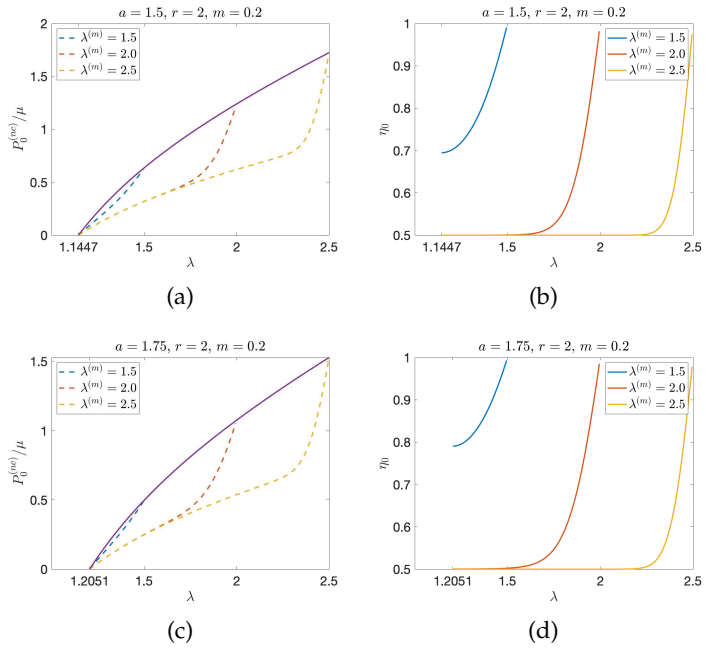

Figure 4. The effect of changing parameter a, showing: (a,c) The scaled values $P_0^{(nc)}/\mu$ of the first Piola-Kirchhoff stress given by (4.9) and (b,d) the damage function η_0 defined by (4.7) when $r = 2$ and $m = 0.2$. In (a,c), the solid curve is for the primary loading, and dashed curves for the unloading from different values of the maximum stretch ratio $\lambda^{(m)}$.

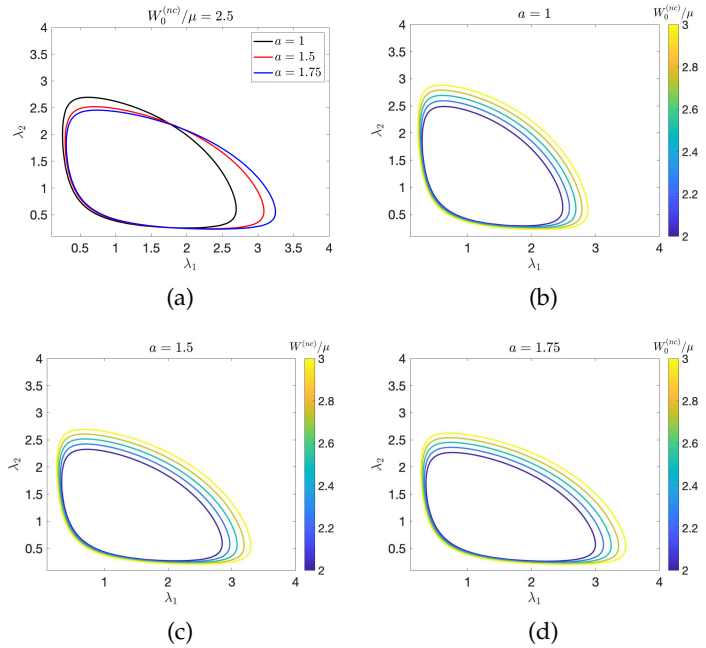

Figure 5. Constant energy contour curves in the (λ_1, λ_2)-plane for the strain-energy given by (3.9) with scaled values $W_0^{(nc)}/\mu \in \{2, 2.25, 2.5, 2.75, 3\}$, when $a \in \{1, 1.5, 1.75\}$. In (a) $W_0^{(nc)}$ is fixed and a varies, while in (b,c,d) a is fixed and $W_0^{(nc)}$ varies.

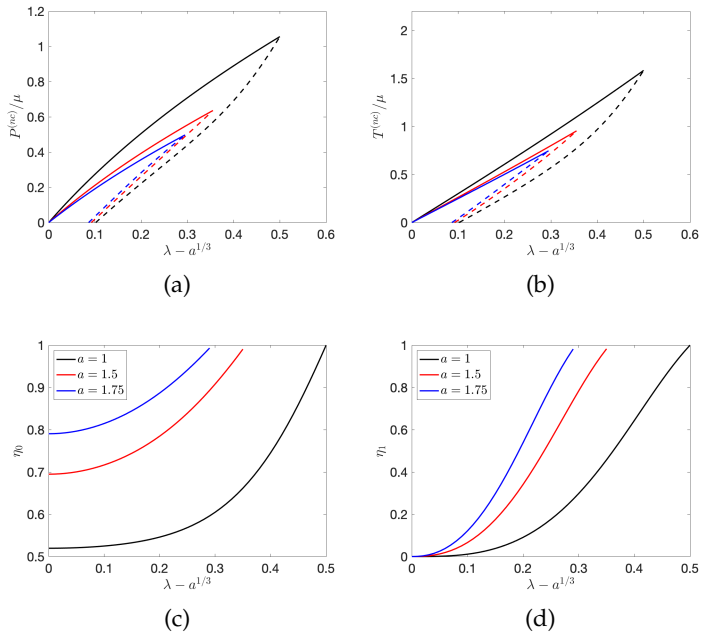

Figure 6. The effect of varying parameter a when unloading begins at maximum stretch ratio $\lambda^{(m)} = 1.5$, showing: (a) The scaled values $P^{(nc)}/\mu$ of the first Piola-Kirchhoff stress given by (4.13); (b) The scaled values $T^{(nc)}/\mu$ of the Cauchy stress given by (4.14); (c) the function η_0 defined by (4.7), with $r = 2$ and $m = 0.2$; and (d) the function η_1 defined by (4.12), with $C_1 = 0.5\left[1 - \text{erf}\left(\lambda^{(m)} - 1\right)\right]$, $C_2 + C_3 = 1$ and $p = 1 + W_0^{(nc)}\left(\lambda^{(m)}, \mathbf{n}\right)/\mu$. In (a,b), solid curves are for primary loading and dashed curves for unloading.

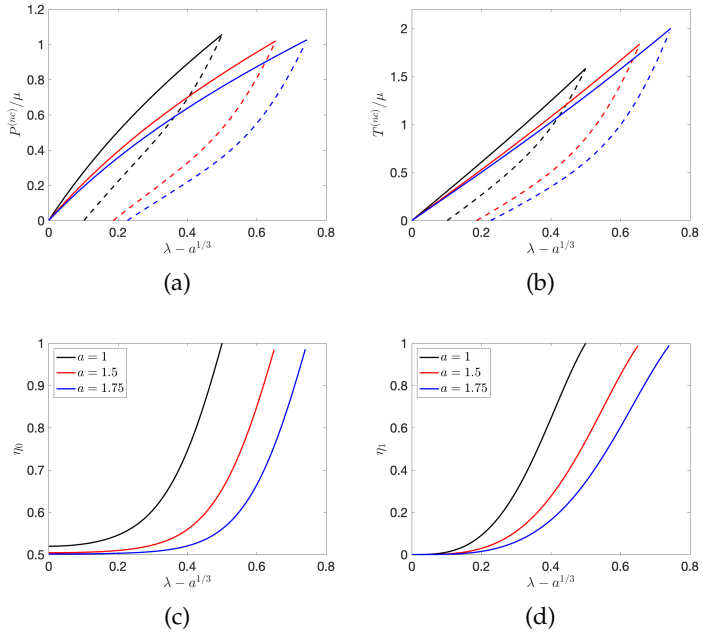

Figure 7. The effect of varying parameter a when unloading starts from a maximum load $P^{(nc)}/\mu \approx 1$, showing: (a) The scaled values $P^{(nc)}/\mu$ of the first Piola-Kirchhoff stress given by (4.13); (b) The scaled values $T^{(nc)}/\mu$ of the Cauchy stress given by (4.14); (c) the function η_0 defined by (4.7), with $r = 2$ and $m = 0.2$; and (d) the function η_1 defined by (4.12), with $C_1 = 0.5\left[1 - \text{erf}\left(\lambda^{(m)} - 1\right)\right]$, $C_2 + C_3 = 1$ and $p = 1 + W_0^{(nc)}\left(\lambda^{(m)}, \mathbf{n}\right)/\mu$. In (a,b), solid curves are for primary loading and dashed curves for unloading.

closed contour in the (λ_1, λ_2)-plane. In Figure 5, contours of scaled constant values of $W_0^{(nc)} = W_0^{(nc)}(\lambda_1, \lambda_2, \mathbf{n})$, defined by (3.9), are plotted in the (λ_1, λ_2)-plane, showing that these contours are convex. Each contour represents a damage threshold, with $\eta_0 = 1$ at any point on the contour. Inside a contour, $\eta_0 < 1$ and no further damage occurs, while crossing the contour will lead to further damage.

(b) Residual strain

When both η_0 and η_1 are active, by (3.27), we have

$$\eta_1(\lambda, \mathbf{n}) = \frac{1}{\operatorname{erf}(1)} \operatorname{erf}\left(\left(\frac{W_0^{(nc)}(\lambda, \mathbf{n})}{W_0^{(nc)}\left(\lambda^{(m)}, \mathbf{n}\right)} \right)^p \right), \tag{4.11}$$

and, by (3.30) and (4.3), we obtain

$$\eta_1(\lambda, \mathbf{n}) = \frac{1}{\operatorname{erf}(1)} \operatorname{erf}\left(\left(\frac{\frac{\lambda^2}{a^{2/3}} + 2\lambda^{-1} a^{1/3} - 3}{\frac{\left(\lambda^{(m)}\right)^2}{a^{2/3}} + 2\left(\lambda^{(m)}\right)^{-1} a^{1/3} - 3} \right)^p \right). \tag{4.12}$$

For uniaxial tension, the function $\phi_1^{(nc)}$ is given implicitly in (4.2).

The first Piola-Kirchhoff stress for the model combining stress softening and residual strain takes the form

$$P^{(nc)} = a^{-1/3} P = \eta_0 \mu a^{1/3} \left(\frac{\lambda}{a} - \lambda^{-2} \right) + (1 - \eta_1)\, a^{1/3} \left(C_1 \frac{\lambda}{a} - \frac{C_2 + C_3}{2} \lambda^{-2} \right). \tag{4.13}$$

The corresponding Cauchy stress is equal to

$$T^{(nc)} = T = \eta_0 \mu a^{1/3} \left(\frac{\lambda^2}{a} - \lambda^{-1} \right) + (1 - \eta_1)\, a^{1/3} \left(C_1 \frac{\lambda^2}{a} - \frac{C_2 + C_3}{2} \lambda^{-1} \right). \tag{4.14}$$

In Figures 6-7, we plot examples of the scaled values $P^{(nc)}/\mu$ and $T^{(nc)}/\mu$ of the first Piola-Kirchhoff stress given by (4.13) and of the Cauchy stress given by (4.14), respectively, of the damage function η_0 defined by (4.7), and of the function η_1 for the residual strain defined by (4.12). In Figure 6, unloading is initiated at a maximum value of the stretch ratio, $\lambda^{(m)} = 1.5$, while in Figure 7, this is from a maximum load value of $P^{(nc)}/\mu \approx 1$. The energy dissipated during a loading-unloading cycle is represented by the hysteretic area for the Cauchy stress.

5. Model example calibrated to data

Stress softening and the accumulated residual strain was assessed systematically in [49], where experimental results for main-chain polydomain LCE samples under cyclic uniaxial tension at different temperatures were presented. For each sample, the mechanism for stress softening was mostly attributed to the change in the microstructure during the polydomain-monodomain transition upon uniaxial loading, and material viscosity. Nevertheless, at 89°C, the LCE behaved like rubber, with the initial cycle exhibiting a slight stress softening and a small set strain, which did not increase with further cycling. This behaviour was considered to be consistent with the Mullins effect, and it was posited that the same inelastic effect could also explain the set strain produced in the first cycle at 62°C. The data sets presented in [49] are therefore suitable candidates to verify the performance of the pseudo-energy function defined by (3.5). Since, due to the polydomain configuration, the nonlinear responses of the LCEs tested under large loads at different temperatures differed both qualitatively and quantitatively, we calibrate our phenomenological model to data corresponding to individual temperatures separately.

During calculations, we have found that the neo-Hookean-based model given by (3.6) is insufficient to capture the complex nonlinear deformation on each loading path, and replaced

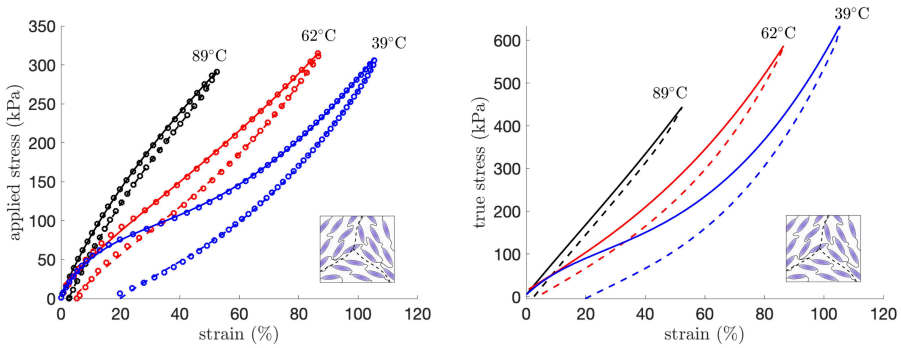

Figure 8. (a) Comparison of computed applied stress vs. strain for the calibrated pseudo-energy function given by (3.5) and the experimental data plotted in Figure 2(b) of [49]; (b) Computed Cauchy stress vs. strain. The base polymeric network is described by a four-parameter Ogden model described by (5.1), while the auxiliary function accounting for residual strain is given by (4.4). Solid and dashed curves are for the computed loading and unloading paths, respectively, and circles for the data. The calibrated model parameters at each temperature are provided in Table 1.

it with a four-term (four-parameter) Ogden-type strain-energy function of the form

$$W_0^{(nc)}(\lambda_1,\lambda_2,\lambda_3,\mathbf{n}) = \frac{\mu_1}{2}\left[a^{1/3}\left(\frac{\lambda_1^2}{a}+\lambda_2^2+\lambda_3^2\right)-3\right]+\frac{\mu_2}{2}\left[a^{-1/3}\left(\lambda_1^{-2}a+\lambda_2^{-2}+\lambda_3^{-2}\right)-3\right]$$
$$+\frac{\mu_3}{8}\left[a^{2/3}\left(\frac{\lambda_1^4}{a^2}+\lambda_2^4+\lambda_3^4\right)-3\right]+\frac{\mu_4}{8}\left[a^{-2/3}\left(\lambda_1^{-4}a^2+\lambda_2^{-4}+\lambda_3^{-4}\right)-3\right], \tag{5.1}$$

where $\{\mu_i\}_{i=1,2,3,4}$ are constants, $\mu=\sum_{i=1}^4\mu_i>0$ is the shear modulus for the polymeric network at small strains [50], and $\{\lambda_i\}_{i=1,2,3}$ satisfy the uniaxial tension condition (4.1). By comparison with our four-parameter model, in [24], a three-term six-parameter Ogden strain-energy function is calibrated to data for particle-reinforced rubber. The function $W_1^{(nc)}$ described by (4.4) remains adequate as auxiliary function.

For our model example, the first Piola-Kirchhoff stress in uniaxial tension takes the form

$$P^{(nc)} = \eta_0\left[\mu_1 a^{1/3}\left(\frac{\lambda}{a}-\lambda^{-2}\right)-\mu_2 a^{-1/3}\left(\lambda^{-3}a-1\right)\right.$$
$$\left.+\frac{\mu_3}{4}a^{2/3}\left(\frac{\lambda^3}{a^2}-\lambda^{-3}\right)-\frac{\mu_4}{4}a^{-2/3}\left(\lambda^{-5}a^2-\lambda\right)\right]+(1-\eta_1)\,a^{1/3}\left(C_1\frac{\lambda}{a}-\frac{C_2+C_3}{2}\lambda^{-2}\right). \tag{5.2}$$

The corresponding Cauchy stress is equal to

$$T^{(nc)} = \eta_0\left[\mu_1 a^{1/3}\left(\frac{\lambda^2}{a}-\lambda^{-1}\right)-\mu_2 a^{-1/3}\left(\lambda^{-2}a-\lambda\right)\right.$$
$$\left.+\frac{\mu_3}{4}a^{2/3}\left(\frac{\lambda^4}{a^2}-\lambda^{-2}\right)-\frac{\mu_4}{4}a^{-2/3}\left(\lambda^{-4}a^2-\lambda^2\right)\right]+(1-\eta_1)\,a^{1/3}\left(C_1\frac{\lambda^2}{a}-\frac{C_2+C_3}{2}\lambda^{-1}\right). \tag{5.3}$$

To calibrate the model parameters, we employed a nonlinear least squares procedure (`lsqnonlin.m`) implemented in *Matlab*. At each temperature, the calibration was realised in two steps. In the first step, the coefficients of the Ogden-type strain-energy function were adjusted to the data along the primary loading path. These coefficients were input parameters for the second

Table 1. Computed parameter values of the pseudo-energy function described by (3.5) calibrated to experimental data plotted in Figure 2(b) of [49]. A comparison between the numerical and experimental results is presented in Figure 8(a).

Temperature	Coefficients of $W_0^{(nc)}$ given by (5.1) and shear modulus μ (kPa)	Coefficients of $W_1^{(nc)}$ given by (4.4)	Parameters of η_0 given by (4.6)	Parameter of η_1 given by (4.11)
89°C	$\mu_1 = 193.6043$, $\mu_2 = 204.2571$ $\mu_3 = 30.5968$, $\mu_4 = 0$ $\mu = \sum_{i=1}^{4} \mu_i = 428.4582$	$C_1 = -1.1553$ $(C_2 + C_3)/2 = 25.9192$	$r = 597.4134$ $m = 0.0012$	$p = 9.0895$
62°C	$\mu_1 = 69.3951$, $\mu_2 = 85.9516$ $\mu_3 = 61.3268$, $\mu_4 = 0$ $\mu = \sum_{i=1}^{4} \mu_i = 216.5735$	$C_1 = 2.6967$ $(C_2 + C_3)/2 = 29.0940$	$r = 5.6174$ $m = 0.6824$	$p = 141.9146$
39°C	$\mu_1 = -57.0148$, $\mu_2 = -328.9884$ $\mu_3 = 91.5032$, $\mu_4 = 626.1964$ $\mu = \sum_{i=1}^{4} \mu_i = 331.7064$	$C_1 = 7.7678$ $(C_2 + C_3)/2 = 108.0556$	$r = 0.5118$ $m = 12.2572$	$p = 113.2093$

step, where all the other material constants were fitted to the data on the unloading path. The computed parameter values are recorded in Table 1. The numerical results for the applied stress, given by (5.2), are compared with the data in Figure 8(a), where an excellent agreement between theory and experiments is found. The corresponding values of the true stress, given by (5.3), are plotted in Figure 8(b), showing the hysteretic energy dissipation in each case. We see that both the loss of energy and the set strain are negligible at 89°C, but increase significantly as temperature decreases from 62°C to 39°C. In Table 1, the coefficient μ_4 vanishes for LCE tested at 89°C and 62°C where reversible deformation mechanisms were observed. For rubber-like material, three-term (three-parameter) Ogden models were calibrated to uniaxial tensile data in [28]. The fact that an extra parameter ($\mu_4 \neq 0$) is required at 39°C may be due to the additional viscous effects which also play a role at this temperature. In contrast, at 62°C, reorientation in the microscopic texture was the dominant mechanism in the first cycles. For a full explanation of the experimental set-up, results and discussion, we refer to [49]. Viscoelastic responses of main-chain polydomain LCEs in loading-unloading uniaxial tensile tests were also demonstrated in [5]. The stress-strain curves displaying stress softening and set strain at various temperatures in Figure 6 of [5] are comparable to those in Figure 2(b) of [49].

6. Conclusion

The neoclassical model, based on the rubber elasticity theory, has been widely used for modelling the mechanical behaviour of nematic elastomers, but cannot account for various inelastic effects displayed by these materials under certain loading conditions. In liquid crystal elastomers (LCEs), these effects are caused by significant microstructural changes under combined loading and optothermal stimuli, and are relevant to important applications, such as mechanical damping and self-healing. Here, we have formulated a *phenomenological pseudo-energy function* for the constitutive modelling of nematic elastomers exhibiting stress softening with residual strain under cyclic loads. To accomplish this, we combined the neoclassical theory with the pseudo-elasticity framework for particle-reinforced rubber proposed in [24,63]. Since uniaxial stretch deformations are easier to reproduce in practice [5,49,53,54], we analysed theoretically the stress softening under cyclic uniaxial tensile loads, and calibrated a specific form of the pseudo-energy function to recent experimental data at various temperatures reported in [49]. Based on our numerical results, we conclude that the pseudo-energy function captures well the Mullins-like inelastic responses observed experimentally in LCEs, but that different parameter sets must be used at different temperatures. Essentially, the material behaves at each temperature as a different LCE material that cannot be simply captured by a modification of the temperature-dependent

nematic parameter a in the neoclassical model. For a fixed temperature, the general model is applicable also to nematic materials under multiaxial loads for which further experimental testing is needed.

Data Accessibility. This paper has no data.

Authors' Contributions. LAM and AG conceived of and designed the study. LAM contributed to the theoretical analysis, performed the numerical calculations and drafted the manuscript. AG contributed to the theoretical analysis, and helped draft the manuscript. **Both the authors gave final approval for publication and agree to be held accountable for the work performed therein.**

Competing Interests. The authors declare that they have no competing interests.

Funding. The support by the Engineering and Physical Sciences Research Council of Great Britain under research grants EP/R020205/1 to Alain Goriely and EP/S028870/1 to L. Angela Mihai is gratefully acknowledged.

Acknowledgements. We are grateful to Prof. Carl P. Frick and Dr Rajib K. Shaha (University of Wyoming) for providing us with the experimental data from their published article [49].

References

1. Agostiniani V, Dal Maso G, DeSimone A. 2015. Attainment results for nematic elastomers, Proceedings of the Royal Society of Edinburgh A 145, 669-701 (doi: 10.1017/S0308210515000128).
2. Agostiniani V, DeSimone A. 2012. Ogden-type energies for nematic elastomers. International Journal of Non-Linear Mechanics 47(2), 402-412 (doi: 10.1016/j.ijnonlinmec.2011.10.001).
3. Agrawal A, Chipara AC, Shamoo Y, Patra PK, Carey BJ, Ajayan PM, Chapman WG, Verduzzo R. 2013. Dynamic self-stiffening in liquid crystal elastomers, Nature Communications 4, 1739 (doi: 10.1038/ncomms2772).
4. Anderson DR, Carlson DE, Fried E. 1999. A continuum-mechanical theory for nematic elastomers, Journal of Elasticity 56, 33-58 (doi: 10.1023/A:1007647913363).
5. Azoug A, Vasconcellos V, Dooling J, Saed M, Yakacki CM, Nguyen TD. 2016., Viscoelasticity of the polydomain-monodomain transition in main-chain liquid crystal elastomers, Polymer 98, 165-171 (doi: 10.1016/j.polymer.2016. 06.022).
6. Beatty MF, Krishnaswamy S. 2000. A theory of stress-softening in incompressible isotropic materials, Journal of the Mechanics and Physics of Solids 48(9), 1931-1965 (doi: 10.1016/S0022-5096(99)00085-X).
7. Benoit W. 2005. Mechanical properties: Anelasticity, Encyclopedia of Condensed Matter Physics, 271-280 (doi: 10.1016/B0-12-369401-9/00574-X).
8. Biggins JS, Warner M. 2009. Supersoft elasticity in polydomain nematic elastomers, Physical Review Letters 103, 037802 (doi: 10.1103/PhysRevLett.103.037802).
9. Biggins JS, Warner M, Bhattacharya. 2012. Elasticity of polydomain liquid crystal elastomers, Journal of the Mechanics and Physics of Solids 60, 573-590 (doi: 10.1016/j.jmps.2012.01.008).
10. Bladon P, Terentjev EM, Warner M. 1994. Deformation-induced orientational transitions in liquid crystal elastomers, Journal de Physique II 4, 75-91 (doi: 10.1051/jp2:1994100).
11. Bouasse H, Carriére Z. 1903. Sur les courbes de traction du caoutchouc vulcanisé, Annales de la Faculté des sciences de Toulouse: Mathématiques, Serie 2, 5 (3), 257-283.
12. Budday S, Sommer G, Birkl C, Langkammer C, Haybäck J, Kohnert J, Bauer M, Paulsen F, Steinmann P, Kuhl E, Holzapfel GA. 2017. Mechanical characterization of human brain tissue, Acta Biomaterialia, 48, 319-340 (doi: 10.1016/j.actbio.2016.10.036).
13. Cirak F, Long Q, Bhattacharya K, Warner M. 2014. Computational analysis of liquid crystalline elastomer membranes: Changing Gaussian curvature without stretch energy, International Journal of Solids and Structures 51(1), 144-153 (doi: 10.1016/j.ijsolstr.2013.09.019).
14. Clarke SM, Terentjev EM, Kundler I, Finkelmann H. 1998. Texture evolution during the polydomain-monodomain transition in nematic elastomers, Macromolecules 31(15), 4862-4872 (doi: 10.1021/ma980195j).
15. DAmbrosio P, De Tommasi D, Ferri D, Puglisi G. 2008. A phenomenological model for healing and hysteresis in rubber-like materials, International Journal of Engineering Science 46(4), 293-305 (doi: 10.1016/j.ijengsci.2007.12.002).
16. de Gennes PG. 1975. Physique moléculaire - réflexions sur un type de polymères nématiques, Comptes rendus de l'Académie des Sciences B 281, 101-103.

17. de Haan LT, Schenning AP, Broer DJ. 2014. Programmed morphing of liquid crystal networks, Polymer 55(23), 5885-5896 (doi: 10.1016/j.polymer.2014.08.023).
18. DeSimone A. 1999. Energetics of fine domain structures, Ferroelectrics 222(1), 275-284 (doi: 10.1080/00150199908014827).
19. DeSimone A, Dolzmann G. 2000. Material instabilities in nematic elastomers, Physica D 136(1-2), 175-191 (doi: S0167-2789(99)00153-0).
20. DeSimone A, Dolzmann G. 2002. Macroscopic response of nematic elastomers via relaxation of a class of SO(3)-invariant energies, Archive of Rational Mechanics and Analysis 161, 181-204 (doi: 10.1007/s002050100174).
21. DeSimone A, Teresi L. 2009. Elastic energies for nematic elastomers, The European Physical Journal E 29, 191-204 (doi: 10.1140/epje/i2009-10467-9).
22. Diani J, Fayolle B, Gilormini P. 2009. A review on the Mullins effect, European Polymer Journal 45, 601-612 (doi: 10.1016/j.eurpolymj.2008.11.017).
23. Dorfmann A. 2003. Stress softening of elastomers in hydrostatic tension, Acta Mechanica 165, 117-137 (doi: 10.1007/s00707-003-0034-5).
24. Dorfmann A, Ogden RW. A constitutive model for the Mullins effect with permanent set in particle-reinforced rubber, International Journal of Solids and Structures 41(7), 1855-1878 (doi: 10.1016/j.ijsolstr.2003.11.014).
25. Dorfmann AL, Woods WA, Trimmer BA. 2008. Muscle performance in a soft-bodied terrestrial crawler: constitutive modeling of strain-rate dependency, Journal of the Royal Society Interface 5, 336-349 (doi: 10.1098/rsif.2007.1076).
26. Eckart C. 1948. The thermodynamics of irreversible processes. IV. The theory of elasticity and anelasticity, Physical Review 73(4), 373-382 (doi: 10.1103/PhysRev.73.373).
27. Finkelmann H, Kock HJ, Rehage G. 1981. Investigations on liquid crystalline polysiloxanes 3, Liquid crystalline elastomers - a new type of liquid crystalline material, Die Makromolekulare Chemie, Rapid Communications 2, 317-322 (doi: 10.1002/marc.1981.030020413).
28. Fitt D, Wyatt H, Woolley TE, Mihai LA. 2019. Uncertainty quantification of elastic material responses: testing, stochastic calibration and Bayesian model selection, Mechanics of Soft Materials 1, 13 (doi: 10.1007/s42558-019-0013-1).
29. Fried E, Sellers S. 2004. Free-energy density functions for nematic elastomers, Journal of the Mechanics and Physics of Solids 52(7), 1671-1689 (doi: 10.1016/j.jmps.2003.12.005).
30. Fung YC. 1980. On the pseudo-elasticity of living tissues, In Mechanics today (ed. S. N. Nasser), Ch. 4, 49-66, Pergamon, New York.
31. Goriely A. 2017. The Mathematics and Mechanics of Biological Growth, Springer-Verlag, New York.
32. Govindjee S, Simo J. 1991. A micro-mechanically based continuum damage model for carbon black filled rubbers incorporating the Mullins effect, Journal of the Mechanics and Physics of Solids 39(1), 87-112 (doi: 10.1016/0022-5096(91)90032-J).
33. Horgan CO, Ogden RW, Saccomandi G. 2004. A theory of stress softening of elastomers based on finite chain extensibility, Proceedings of the Royal Society A 460, 1737-1754 (doi: 10.1098/rspa.2003.1248).
34. Horgan CO, Saccomandi G. 2004. Constitutive models for compressible nonlinearly elastic materials with limiting chain extensibility, Journal of Elasticity 77, 123-138 (doi: 10.1007/s10659-005-4408-x).
35. Jiang ZC, Xiao YY, Zhao Y. 2019. Shining light on liquid crystal polymer networks: preparing, reconfiguring, and driving soft actuators, Advanced Optical Materials 7, 1900262 (doi: 10.1002/adom.201900262).
36. Johnson M, Beatty M. 1993. The Mullins effect in uniaxial extension and its influence on the transverse vibration of a rubber string, Continuum Mechanics and Thermodynamics 5, 83-115 (doi: 10.1007/BF01141446).
37. Johnson MA, Beatty MF. 1995. The Mullins effect in equibiaxial extension and its influence on the inflation of a balloon, International Journal of Engineering Science 33(2), 223-245 (doi: 10.1016/0020-7225(94)E0052-K).
38. Kuenstler AS. Hayward RC. 2019. Light-induced shape morphing of thin films, Current Opinion in Colloid & Interface Science 40, 70-86 (doi: 10.1016/j.cocis.2019.01.009).
39. Küpfer J, Finkelmann H. 1991. Nematic liquid single crystal elastomers, Die Makromolekulare Chemie, Rapid Communications 12, 717-726 (doi: 10.1002/marc.1991.030121211).
40. Lazopoulos KA, Ogden RW. 1998. Nonlinear elasticity theory with discontinuous internal variables, Mathematics and Mechanics of Solids 3, 29-51 (doi: 10.1177/108128659800300103).

41. Leblanc JL. 2010. Filled Polymers: Science and Industrial Applications, CRC Press, Taylor & Francis Group, Boca Raton, USA.
42. Li Z, Xu H, Xia X, Song Y, Zheng Q. 2019. Energy dissipation accompanying Mullins effect of nitrile butadiene rubber/carbon black nanocomposites, Polymer 171, 106-114 (doi: 10.1016/j.polymer.2019.03.043).
43. Lubarda VA. 2004. Constitutive theories based on the multiplicative decomposition of deformation gradient: thermoelasticity, elastoplasticity and biomechanics, Applied Mechanics Reviews 57(2), 95-108 (doi: 10.1115/1.1591000).
44. Machado G, Chagnon G, Favier D. 2012. Induced anisotropy by the Mullins effect in filled silicone rubber, Mechanics of Materials 50, 70-80 (doi: 10.1016/j.mechmat.2012.03.006).
45. Mao Y, Warner M, Terentjev EM, Ball RC. 1998. Finite extensibility effects in nematic elastomers, The Journal of Chemical Physics 108, 8743-8748 (doi: 10.1063/1.476303).
46. Martinoty P, Stein P, Finkelmann H, Pleiner H, Brand HR. 2004. Mechanical properties of monodomain side chain nematic elastomers,The European Physical Journal E 14, 311-321(doi: 10.1140/epje/i2003-10154-y).
47. Maugin GA. 2003. Pseudo-plasticity and pseudo-inhomogeneity effects in materials mechanics, Journal of Elasticity 71, 81âĂŞ103 (doi: 10.1023/B:ELAS.0000005634.81007.11).
48. McCracken JM, Donovan BR, White TJ. 2020. Materials as Machines, Advanced Materials 32, 1906564 (doi: 10.1002/adma.201906564).
49. Merkel DR, Shaha RK, Yakacki CM, Frick CP. 2019. Mechanical energy dissipation in polydomain nematic liquid crystal elastomers in response to oscillating loads, Polymer 166, 148-154 (doi: 10.1016/j.polymer.2019.01.042).
50. Mihai LA, Goriely A. 2017. How to characterize a nonlinear elastic material? A review on nonlinear constitutive parameters in isotropic finite elasticity, Proceedings of the Royal Society A 473, 20170607 (doi: 10.1098/rspa.2017.0607).
51. Mihai LA, Goriely A. 2020. Likely striping in stochastic nematic elastomers, Mathematics and Mechanics of Solids 25(10), 1851-1872 (doi: 0.1177/1081286520914958).
52. Mihai LA, Goriely A. 2020. A plate theory for nematic liquid crystalline solids, Journal of the Mechanics and Physics of Solids (doi: 10.1016/j.jmps.2020.104101).
53. Mistry D, Gleeson HF. 2019. Mechanical deformations of a liquid crystal elastomer at director angles between 0° and 90°: Deducing an empirical model encompassing anisotropic nonlinearity, Journal of Polymer Science 57, 1367-1377 (doi: 0.1002/polb.24879).
54. Mistry D, Nikkhou M, Raistrick T, Hussain M, Jull EIL, Baker DL, Gleeson HF. 2020. Isotropic liquid crystal elastomers as exceptional photoelastic strain sensors, Macromolecules 53, 3709-3718 (doi: 10.1021/acs.macromol.9b02456).
55. Mullins L. 1948. Effect of stretching on the properties of rubber, Rubber Chemistry and Technology 21(2), 281-300 (doi: 10.5254/1.3546914).
56. Mullins L. 1949. Permanent set in vulcanized rubber, Rubber Chemistry and Technology 22(4), 1036-1044 (doi: 10.5254/ 1.3543010).
57. Mullins L. 1969. Softening of rubber by deformation, Rubber Chemistry and Technology 42(1), 339-362 (doi: 10.5254/1.3539210).
58. Mullins L, Tobin NR. 1957. Theoretical model for the elastic behaviour of filler-reinforced vulcanized rubbers, Rubber Chemistry and Technology 30(2), 555-571 (doi: 10.5254/1.3542705).
59. Mullins L, Tobin NR. 1965. Stress softening in rubber vulcanizates. part I. Use of a strain amplification factor to describe the elastic behavior of filler-reinforced vulcanized rubber, Journal of Applied Polymer Science 9(9), 2993-3009 (doi: 10.1002/app.1965.070090906).
60. Muñoz MJ, Bea JA, Rodríguez JF, Ochoa I, Grasa J, Pérez del Palomar A, Zaragoza P, Osta R, Doblaré. 2008. An experimental study of the mouse skin behaviour: damage and inelastic aspects, Journal of Biomechanics 41(1), 93-99 (doi: 10.1016/j.jbiomech.2007.07.013).
61. Neubert D, Saunders DW. 1958. Some observations of the permanent set of cross-linked natural rubber samples after heating in a state of pure shear, Rheologica Acta 1, 151-157 (doi: 10.1007/BF01968858).
62. Ogden RW. 1997. Non-Linear Elastic Deformations, 2nd ed, Dover, New York.
63. Ogden RW, Roxburgh DG. 1998. A pseudo-elastic model for the Mullins effect in filled rubber, Proceedings of the Royal Society A 455, 2861-2877 (doi: 10.1098/rspa.1999.0431).
64. Pang X, Lv Ja., Zhu C, Qin L, Yu Y. 2019. Photodeformable azobenzene-containing liquid crystal polymers and soft actuators, Advanced Materials, 1904224 (doi: 10.1002/adma.201904224).

65. Rajagopal K, Srinivasa A. 2004. On the thermomechanics of materials that have multiple natural configurations part I, Zeitschrift für angewandte Mathematik und Physik ZAMP 55, 861-893 (doi: 10.1007/s00033-004-4019-6).
66. Rajagopal K, Wineman AS. 1992. A constitutive equation for nonlinear solids which undergo deformation induced microstructural changes, International Journal of Plasticity 8(4), 385-395 (doi: 10.1016/0749-6419(92)90056-I).
67. Rickaby SR, Scott NH. 2013. A cyclic stress softening model for the Mullins effect, International Journal of Solids and Structures 50, 111-120 (doi: 10.1016/j.ijsolstr.2012.09.006).
68. Soni H, Pelcovits RA, Powers TR. 2016. Wrinkling of a thin film on a nematic liquid-crystal elastomer, Physical Review E 94, 012701 (doi: 10.1103/PhysRevE.94.012701).
69. Tobolsky AV. 1960. Properties and Structures of Polymers, John Wiley and Sons, New York, Chap. 5, 223-265.
70. Tobolsky AV, Prettyman IB, Dillon JH. 1944. Stress relaxation of natural and synthetic rubber stocks, Journal of Applied Physics 15, 380-395 (doi: 10.1063/1.1707442).
71. De Tommasi D, Puglisi G, Saccomandi G. 2006. A micromechanics based model for the Mullins effect, Journal of Rheology 50, 495-512 (doi: 10.1122/1.2206706).
72. De Tommasi D, Puglisi G. 2007. Mullins effect for a cylinder under extension and torsion, Journal of Elasticity 86, 85-99 (doi: 10.1007/s10659-006-9087-8).
73. Treloar LRG. 2005. The Physics of Rubber Elasticity, 3rd ed, Oxford University Press, Oxford, UK.
74. Truesdell C, Noll W. 2004. The Non-Linear Field Theories of Mechanics, 3rd ed, Springer-Verlag, New York.
75. Ula SW, Traugutt NA, Volpe RH, Patel RP, Yu K, Yakacki CM. 2018. Liquid crystal elastomers: an introduction and review of emerging technologies, Liquid Crystals Review 6, 78-107 (doi: 10.1080/21680396.2018.1530155).
76. Verwey GC, Warner M, Terentjev EM. 1996. Elastic instability and stripe domains in liquid crystalline elastomers, Journal de Physique 6(9), 1273-1290 (doi: 10.1051/jp2:1996130).
77. Wan G, Jin C, Trase I, Zhao S, Chen Z. 2018. Helical structures mimicking chiral seedpod opening and tendril coiling, Sensors 18(9), 2973 (doi: 10.3390/s18092973).
78. Wang Z, Tian H, He Q, Cai S. 2017. Reprogrammable, reprocessible, and self-healable liquid crystal elastomer with exchangeable disulfide bonds, ACS Applied Materials & Interfaces 9(38), 33119-33128 (doi: 10.1021/acsami.7b09246).
79. Warner M. 2020. Topographic mechanics and applications of liquid crystalline solids, Annual Review of Condensed Matter Physics 11, 125-145 (doi: 10.1146/annurev-conmatphys-031119-050738).
80. Warner M, Bladon P, Terentjev E. 1994. "Soft elasticity" - deformation without resistance in liquid crystal elastomers, Journal de Physique II 4, 93-102 (doi: 10.1051/jp2:1994116).
81. Warner M, Gelling KP, Vilgis TA. 1988. Theory of nematic networks, The Journal of Chemical Physics 88, 4008-4013.
82. Warner M, Terentjev EM. 1996. Nematic elastomers - a new state of matter?, Progress in Polymer Science 21, 853-891.
83. Warner M, Terentjev EM. 2007. Liquid Crystal Elastomers, paper back, Oxford University Press, Oxford, UK.
84. Warner M, Wang, XJ. 1991. Elasticity and phase behavior of nematic elastomers, Macromolecules 24, 4932-4941 (doi: 10.1021/ma00017a033).
85. White TJ, Broer DJ. 2015. Programmable and adaptive mechanics with liquid crystal polymer networks and elastomers, Nature Materials 14, 1087-1098 (doi: 10.1038/nmat4433).
86. Wineman AS, Rajagopal K. 1990. On a constitutive theory for materials undergoing microstructural changes, Archives of Mechanics 42, 53-57.
87. Wineman A, Min JH. 2004. Inhomogeneity in a sheared elastomeric layer as a result of thermally induced scission and healing, Mathematics and Mechanics of Solids 9(1), 17-35 (doi: 0.1177/1081286503035197).
88. Wineman AS, Shaw JA. 2002. Scission and healing in a spinning elastomeric cylinder at elevated temperature, Transactions of the ASME 69, 602-609 (doi: 10.1115/1.1485757).
89. Zener C. 1948. Elasticity and Anelasticity of Metals, University of Chicago Press, Chicago, Illinois.
90. Zhang Y, Xuan C, Jiang Y, Huo Y. 2019. Continuum mechanical modeling of liquid crystal elastomers as dissipative ordered solids, Journal of the Mechanics and Physics of Solids 126, 285-303 (doi: 10.1016/j.jmps.2019.02.018).